Steel and Composite Structures, *Vol. 36, No. 4* (*2020*) *427-446*
DOI: https://doi.org/10.12989/scs.2020.36.4.427

Progressive collapse analysis of stainless steel composite frames with beam-to-column endplate connections

Jia Wang*, Brian Uy[a], Dongxu Li[b] and Yuchen Song[c]

School of Civil Engineering, The University of Sydney, Sydney, NSW, 2006, Australia

(*Received June 24, 2020, Revised July 21, 2020, Accepted July 24, 2020*)

Abstract. This paper carries out the progressive collapse analysis of stainless steel composite beam-to-column joint sub-models and moment-resisting frames under column removal scenarios. The static flexural response of composite joint sub-models with damaged columns was initially explored via finite element methods, which was validated by independent experimental results and discussed in terms of moment-rotation relationships, plastic hinge behaviour and catenary actions. Simplified finite element methods were then proposed and applied to the frame analysis which aimed to elaborate the progressive collapse response at the frame level. Nonlinear static and dynamic analysis were employed to evaluate the dynamic increase factor (DIF) for stainless steel composite frames. The results suggest that the catenary action effect plays an important role in preventing the damaged structure from dramatic collapse. The beam-to-column joints could be critical components that influence the capacity of composite frames and dominate the determination of dynamic increase factor. The current design guidance is non-conservative to provide proper DIF for stainless steel composite frames, and thus new DIF curves are expected to be proposed.

Keywords: progressive collapse; stainless steel; beam-to-column joints; static and dynamic; composite frames

1. Introduction

Progressive collapse risk has been widely discussed within the last decades since the building collapse could lead to catastrophic threats to the safety of life and property. Collapses of building are normally caused by a sudden loss of critical components which could have been designed with sufficient stiffness and load-bearing capacity. In fact, the column removal is regarded as the highest risk that can potentially result in a loss of flexural resistance of beams and thus creates irreparable damages of frames as shown in Fig. 1. Moreover, additional damages could happen in adjacent structures due to dynamic effects, which induces the domino-effect collapse. The catastrophic collapse of World Trade Tower in US has elevated the concerns on the building safety. As a result, more research investigating the structural performance under column removal scenarios could provide valuable insight into the topic.

Currently, a large number of experimental and numerical studies have been reported with a focus on the behaviour of sub-assemblages and frames. Sadek *et al*. (2011) carried out experiments to investigate the static behaviour of beam-to-column joints with the loss of column, in which failure modes and flexural response were observed. It was found that catenary actions played an important role in the plastic response leading to a significant increase in the resistance. Likewise, Yang and Tan (2013) conducted similar static tests of beam-to-column joints but various connection types were included. Meanwhile, the percentage contribution of catenary actions was obtained and assessed among the different kinds of joints. Results suggested that semi-rigid joints exhibited good performance owing to the large rotational capacity. On this basis, Yang *et al*. (2016) further extended the pure steel beam-to-column joint test into composite joints including concrete slabs. They concluded that reinforcing bars could make large contributions to the catenary action effects such that the load-bearing capacity was improved notably. Analytical models were also developed by Yang *et al*. (2015) based on the component method to simplify the predictions. Guo *et al*. (2015) and Xu *et al*. (2018) pointed out that most of the joint tests concerning the column removal scenario in previous literature simplified the boundary conditions by restraining both ends of the beam with pin supports. The pin supports could generate tensile reactions to simulate the catenary actions, however, the set-up rigidly restrained the longitudinal translation of beam tips which might not be equivalent to actual boundary conditions. As such, they tested steel and composite frames with four bays, and experimental outcomes suggested that side columns could experience large bending moments due to the middle column loss. Apart from monotonic loading tests, diverse frame-level tests and simulations were deployed accounting for dynamic effects. Chen *et al*. (2012) experimentally assessed the progressive collapse behaviour of two-storey

*Corresponding author, Ph.D. Research associate
E-mail: jia.wang@sydney.edu.au
[a]Professor
E-mail: brian.uy@sydney.edu.au
[b]Ph.D. Research associate
E-mail: dongxu.li@sydney.edu.au
[c]Ph.D. Student
E-mail: yuchen.song@sydney.edu.au

http://www.techno-press.org/?journal=scs&subpage=8
ISSN: 1229-9367 (Print), 1598-6233 (Online)

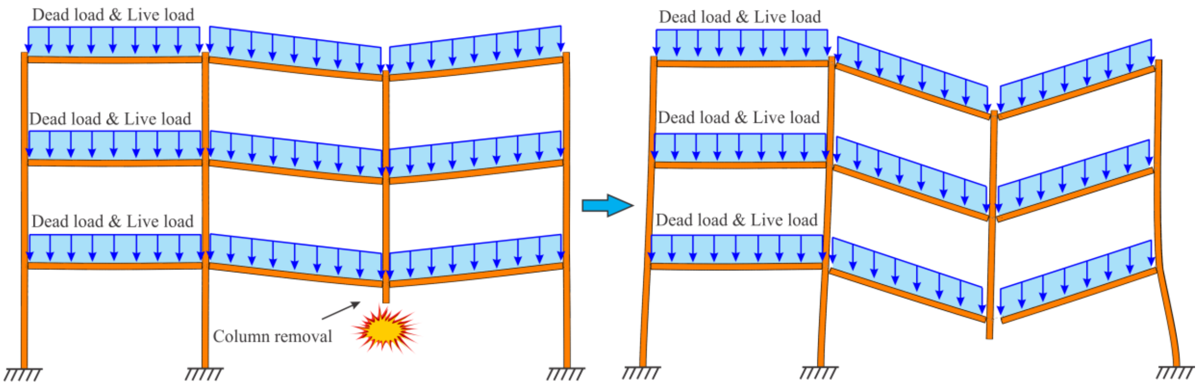

Fig. 1 Typical progressive collapse failure of frames due to a column loss

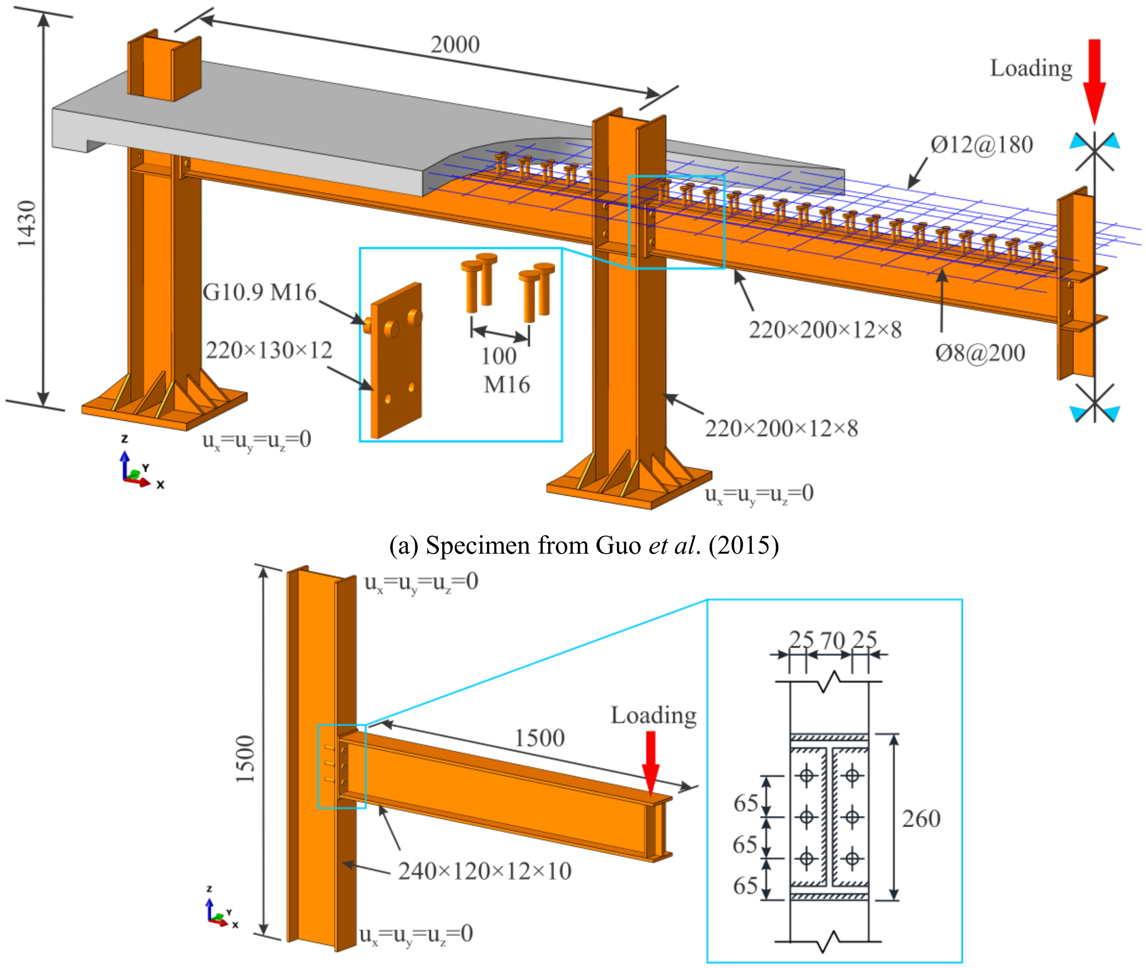

(b) Specimen from Elflah *et al.* (2019)

Fig. 2 Details of beam-to-column joint sub-models (Unit: mm)

and two-bay frames via suddenly removing a middle column. Results showed that vertical displacements approached a certain value with the oscillatory convergence caused by the damping effect. A similar progressive collapse frame test was performed by Li *et al.* (2018) in which dynamic response was captured, and it was found the capacity of connections dominated the flexural behaviour of frames.

It is noted that the aforementioned literature focused on structures fabricated by carbon steels which have been widely applied in structural engineering. However, stainless steels are gaining increasing interest owing to their competitive advantages such as high ductility, significant strain-hardening effect, high resistance in corrosion, etc. Preliminary numerical analysis on composite beam-to-column joints fully made of stainless steels has demonstrated good performance as well (Wang *et al.* 2019,

Table 1 Material property of components

Reference	Component	Young's modulus E_0 (MPa)	Yield strength σ_{ys} / $\sigma_{0.2}$ (MPa)	Ultimate strength σ_{us} (MPa)	Elongation at fracture ε_f (%)	n	m	Compressive strength f_c (MPa)
Guo *et al*. (2015)	Beam flange	196,000	269	401				
	Beam web	209,000	275	411				
	Column flange	200,000	247	396				
	Column web	198,000	276	415				
	Reinforcement (N12)	195,000	331	464				
	Reinforcement (N8)	195,000	325	487				
	G10.9 Bolt	200,000	1067	1186				
	Headed stud*	200,000	235	410				
	Concrete	26,500						26.4 (Cube)
Elflah *et al*. (2019)	Flange	196,500	306	630	66	5.2	2.37	
	Web	205,700	320	651	65	6.7	2.41	
	Endplate	198,000	343	655	54	12.2	2.5	
	Bolt	191,500	617	805	12	17.24	3.68	
Gardner et al. (2016)	Reinforcement	202,600	480	764	38.6			

Note: Factors n and m are exponents related to strain hardening. The material property in headed stud marked with "*" is referred to data in AS 4100 (1998)

Song *et al*. 2019). Therefore, it is desired to further assess the behaviour of stainless steel composite frames, especially the progressive collapse behaviour, since the high ductility is expected to benefit the frame design and avoid instant damages by enhancing the robustness.

In addition, in view of the unpredictable event, it is highly demanded to propose systematically effective provisions so that the survival structures are still capable of providing robust residual capacity to resist further collapse. So far, several design codes and guidance, such as GSA guidelines (2003), UFC 4-023-03 (2009) and ASCE 41-17 (2017), have included the direct or indirect design approaches for the collapse prevention. Alternate Path (AP) method, which is classified as the direct design approach, has been broadly adopted in structural design practice owing to its simple concept and straightforward procedure. It allows the damaged components to bridge over the adjacent members to resist the gravity loads transmitted from the affected bays. The method consists of Linear Static (LS), Nonlinear Static (NS) and Nonlinear Dynamic (ND) analysis in general, and the last method (ND) could more precisely reflect the realistic performance but results in relatively complex works. In this respect, LS and NS analysis is far preferable where an amplification factor can be employed to effectively achieve the equivalent results (Mirtaheri and Zoghi 2016, Mashhadi and Saffari 2016, Cassiano *et al*. 2016). The amplification factor was previously conservatively taken as two until McKay *et al*. (2012) suggested to reduce the value based on allowed and yield deformations. The factor was subsequently modified by Liu (2013) which took the elastic response into consideration. To this end, this study further investigates the dynamic increase factor (DIF) to assess if the current strategy is applicable to stainless steel structures.

Overall, based on the above-mentioned research gap, this paper initially investigated the flexural performance of stainless steel beam-to-column composite joints under the column removal scenarios via finite element methods. The numerical results validated by independent experimental results were thereafter assessed in terms of moment-rotation relationships, plastic hinge and catenary actions. Simplified finite element methods were proposed and applied to the frame analysis which aimed to elaborate the progressive collapse response at the frame level. Consequently, nonlinear static and dynamic analysis were employed to evaluate DIF for stainless steel composite frames, which was expected to provide supplementary support for design guidance.

2. Numerical modelling of joint sub-assemblages

2.1 Development of finite element models

It is noted that the progressive collapse behaviour can be preliminarily assessed via the nonlinear static (NS) analysis on the joint sub-assemblages. This is because the beam-to-column connections are the critical components that govern the flexural response of moment-resisting frames. Moreover, the catenary action effects could be captured if sufficient bays of sub-models are provided. As such, the sub-assemblages were firstly modelled to provide an insight into the static performance of composite joints with column removed.

Three-dimensional numerical models were developed by using Abaqus software (2016) based on the experimental specimens from Guo *et al*. (2015) and Elflah *et al*. (2019). It is noteworthy that the specimen from Guo *et al*. (2015) was made of carbon steel since currently there is a lack of tests concerning stainless steel composite joints. Only stainless steel bolted joints without concrete can be found in Elflah *et al*. (2019). In this respect, both sub-assemblages were adopted to verify the numerical model. The geometrical configuration and material properties are comprehensively illustrated in Fig. 2 and Table 1. Given the geometrical and loading symmetry, a half of sub-model based on the

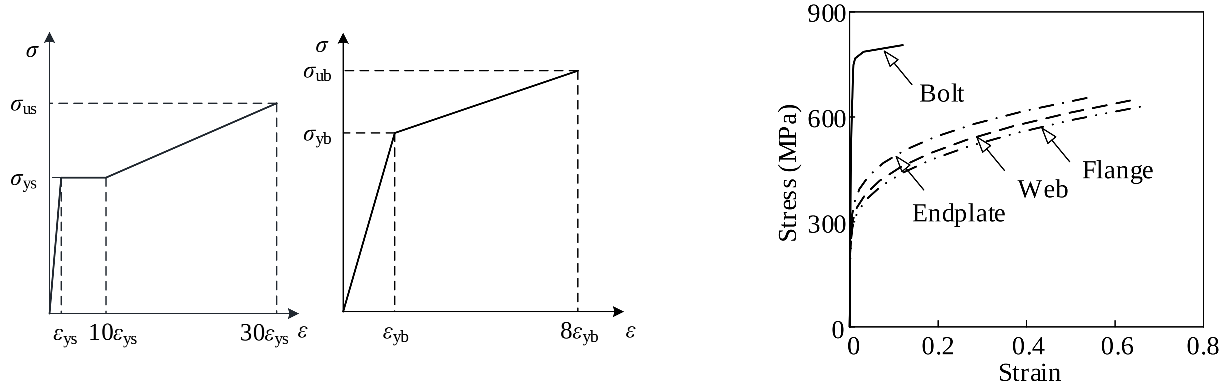

(a) Carbon steel (b) Stainless steel

Fig. 3 Material properties of steel components

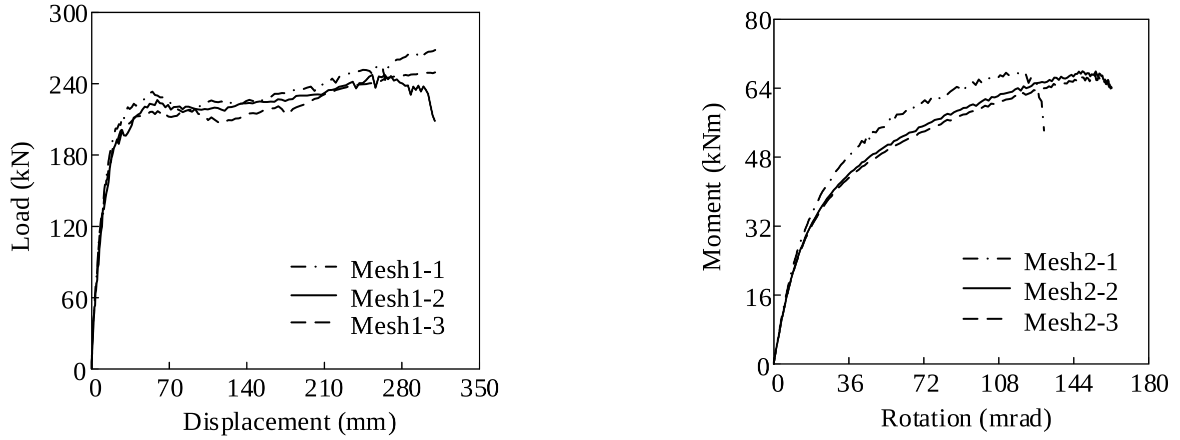

(a) Beam-to-column composite joint sub-assemblage (b) Stainless steel joint

Fig. 4 Mesh convergence analysis

specimen from Guo *et al*. (2015) was created to save computation time. All components were modelled with solid elements (C3D8R) except reinforcing bars which were simulated by truss elements (T3D2).

Quasi-static analysis was performed through the dynamic/explicit solver algorithm to achieve the damage simulation. "General contact" strategy was adopted which offered great convenience for complex interaction conditions since the contact pairs can be detected and generated automatically. Tangential behaviour with a friction coefficient of 0.3 and normal behaviour with hard contact strategy were employed. Additionally, vertical loads were applied under the displacement control as shown in Fig 2. The loading time or step time in the models was selected cautiously to balance the quasi-static accuracy and computation cost. Besides, the pretension of bolts was achieved by applying negative temperature to induce the shrinkage of bolt shanks.

With respect to material properties, stress and strain behaviour was obtained from the related research which is summarised in Table 1. Due to a lack of strain information corresponding to the ultimate strength for the specimen in Guo *et al*. (2015), assumptions were made herein to describe stress-strain relationships of carbon steel components based on the study in Wang *et al*. (2018b), which is denoted in Fig. 3(a). In assumption, the trilinear model was adopted for flanges, webs and reinforcing bars, whereas the bilinear model was applied to bolts. It is noted that the strength of headed stud in the independent literature was not completely provided except for yield strength. In this light, ultimate strength from AS 4100 (1998) was adopted instead. The stress-strain relationships of stainless steel can be expressed as Eqs. (1) and (2), and data were obtained from Elflah *et al*. (2019) plotted in Fig. 3(b).

$$\varepsilon = \frac{\sigma}{E_0} + 0.002(\frac{\sigma}{\sigma_{0.2}})^n, \sigma < \sigma_{0.2} \tag{1}$$

$$\varepsilon = \frac{\sigma - \sigma_{0.2}}{E_{0.2}} + (\varepsilon_u - \varepsilon_{0.2} - \frac{\sigma_u - \sigma_{0.2}}{E_{0.2}}) \times (\frac{\sigma - \sigma_{0.2}}{\sigma_u - \sigma_{0.2}})^m + \varepsilon_{0.2}, \sigma > \sigma_{0.2} \tag{2}$$

where factors n and m are exponents related to strain hardening.

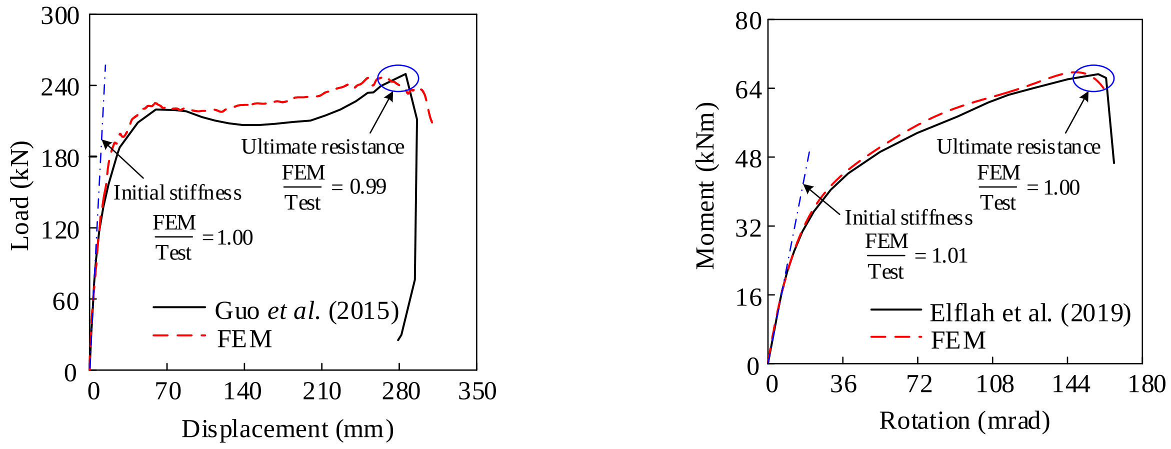

(a) Beam-to-column composite joint sub-assemblage (b) Stainless steel joint

Fig. 5 Verification of numerical results

Table 2 Element size details (Unit: mm)

Model no.	Column	Beam	Endplate	Bolt	Concrete slab	Shear connector
Mesh1-1	35	40	30	15	50	15
Mesh1-2	25	30	20	10	40	10
Mesh1-3	15	20	10	5	30	5
Mesh2-1	30	30	15	8		
Mesh2-2	20	20	10	4		
Mesh2-3	15	15	8	3		

Meanwhile, ductile damage model was included in the material properties to simulate the damage of components, which has been reliably implemented in the previous studies (Wang *et al*. 2018a and Wang *et al*. 2019). Accordingly, the damage initiation and the damage evolution criteria were determined and suggested by Pavlović *et al*. (2014). The equivalent plastic strain at the onset of damage was related to the stress triaxiality and uniaxial plastic strain at the onset of damage as follows

$$\bar{\varepsilon}^{\mathrm{pl}}(\theta)=\varepsilon_{\mathrm{d}}^{\mathrm{pl}}\times\exp[-1.5(\theta-1/3)] \tag{3}$$

where $\varepsilon_{\mathrm{d}}^{\mathrm{pl}}$ is the equivalent plastic strain at the onset of damage; θ is the stress triaxiality.

The damage evolution was defined by determining the equivalent plastic displacement at fracture by Eq. (4)

$$\bar{u}_{\mathrm{f}}^{\mathrm{pl}}=\lambda L_{\mathrm{E}}(\varepsilon_{\mathrm{f}}^{\mathrm{pl}}-\varepsilon_{\mathrm{d}}^{\mathrm{pl}}) \tag{4}$$

where $\bar{u}_{\mathrm{f}}^{\mathrm{pl}}$ is the equivalent plastic displacement at fracture; λ is element size factor of which the final value can be defined by mesh convergence analysis in comparison with the experimental data; L_{E} is characteristic element length, $\varepsilon_{\mathrm{f}}^{\mathrm{pl}}$ is the equivalent plastic strain at fracture.

In addition, the constitutive relationship of concrete was referred to Carreira and Chu (1985) as

$$\frac{\sigma}{f_c}=\frac{\beta(\varepsilon/\varepsilon_c)}{\beta-1+(\varepsilon/\varepsilon_c)^{\beta}} \tag{5}$$

$$\beta=\left(\frac{f_c}{32.4}\right)^3+1.55 \tag{6}$$

$$\varepsilon_c=(0.71f_c+168)\times10^{-5} \tag{7}$$

where f_{c} and ε_{c} is the compressive strength of concrete and the corresponding strain, respectively.

2.2 Verification of numerical results

Mesh convergence analysis was first conducted to determine the appropriate mesh sizes that contributed to an economic computing costs without sacrificing the accuracy. Meanwhile, it can help define parameters related to fracture models in Eq. (4). Three types of models with various element sizes in each sub-assemblage were considered. The detailed element sizes and the corresponding results are outlined in Table 2 and Fig. 4, respectively. It can be seen from the figure that the composite joint sub-assemblage was not evidently sensitive to the mesh size, while premature failure was obtained in the stainless steel model with coarse element sizes. In this light, mesh sizes applied in Mesh1-2 and Mesh2-2 were adopted respectively for the two sub-assemblages.

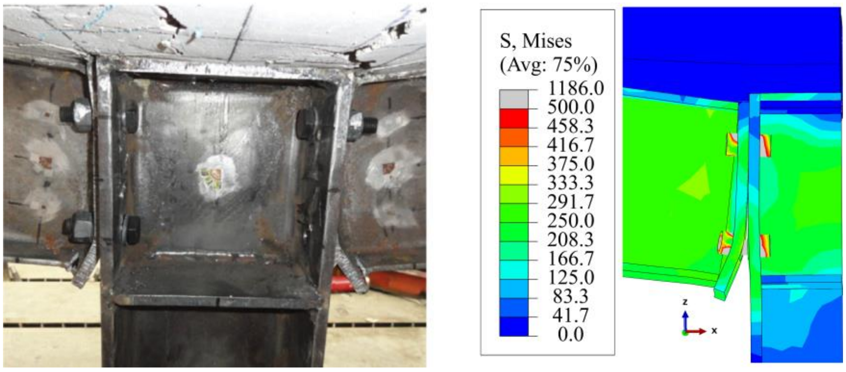

(a) Middle column from Guo *et al*. (2015)

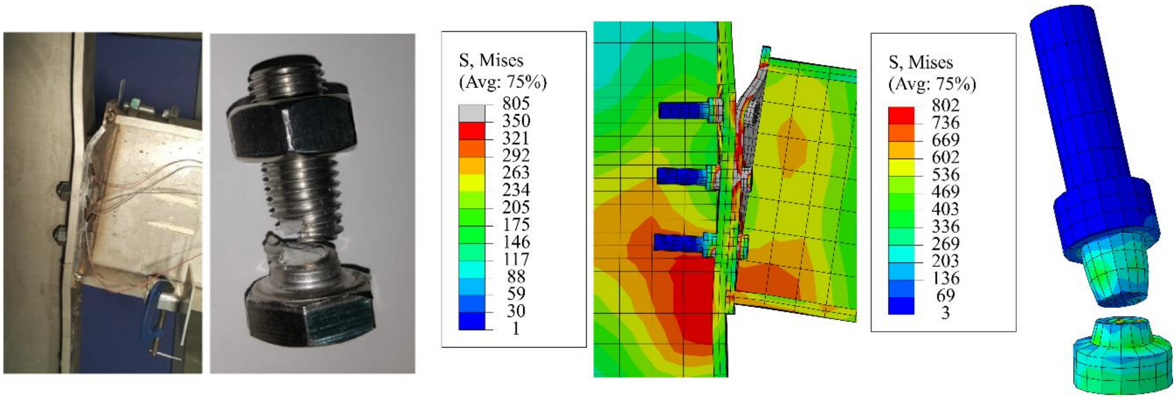

(b) Stainless steel joint from Elflah *et al*. (2019)

Fig. 6 Deformation and damage comparison between specimens and FEM (Unit: MPa)

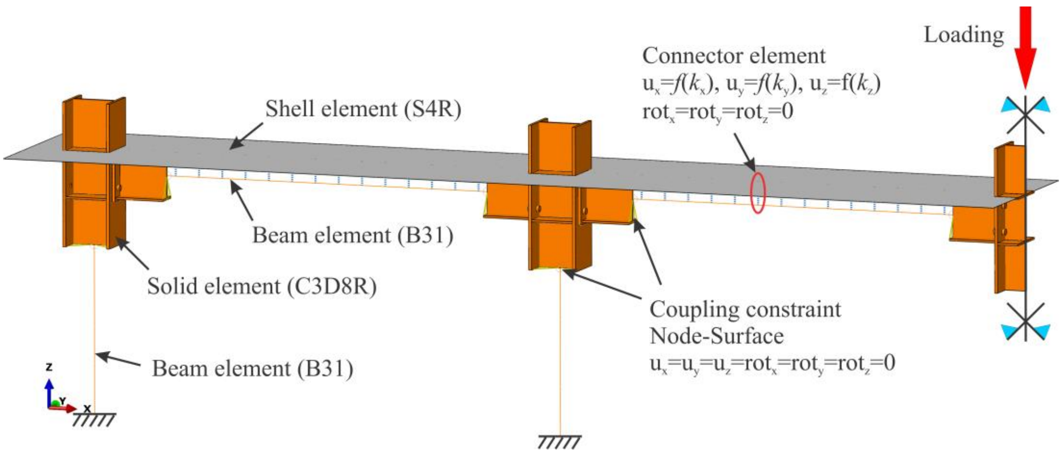

Fig. 7 Simplified beam-to-column joint sub-model

The numerical results obtained from both models were compared with the corresponding experimental curves indicated in Fig. 5. The load and displacement data in Fig. 5(a) were collected from the middle column where vertical loads were applied, while the moment and rotation values in Fig. 5(b) were determined by the deformed endplate. In addition, the deformation and damage patterns are compared in Fig. 6. The comparisons suggested that the finite element method was able to estimate the flexural performance and failure modes with acceptable accuracy. In particular, the prediction ratio related to the initial stiffness and ultimate resistance in both models approached 1, highlighting that the numerical simulations could provide satisfactory prediction in the elastic stage as well as the plastic stage. Note that there existed a slight discrepancy between numerical and experimental results in the specimen from Guo *et al*. (2015), where the experimental curve declined more before rising to the ultimate resistance. It could attribute to the concrete crush and spalling which resulted in an evident reduction in the load-bearing resistance. This phenomenon, however, was not fully reproduced by the adopted concrete model. The concrete-

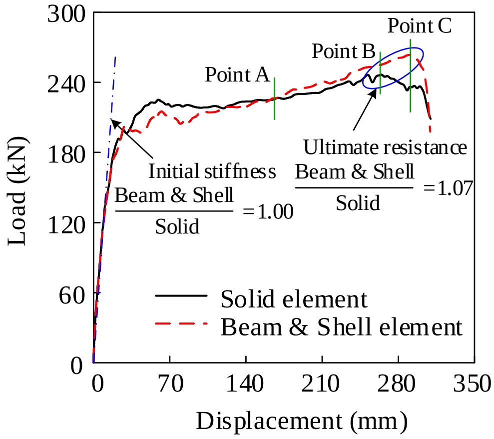

(a) Load-displacement curve

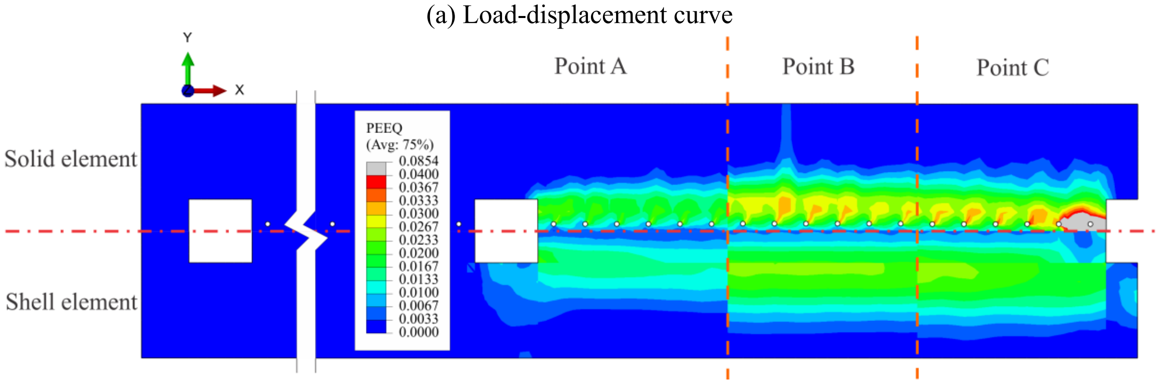

(b) Equivalent plastic strain of concrete slab

Fig. 8 Comparison of numerical results with solid elements and beam & shell elements

related descending curve could be more evident in concrete structures but ignorable in steel structures (Sadek *et al.* 2011). Nonetheless, the discrepancy can be reasonably tolerated in composite structures since the drop in the resistance was subsequently offset by the strain-hardening effects and catenary actions.

2.3 Simplified modelling strategy

Although the solid elements are able to simulate the structural performance relatively precisely, the great demand for computation costs hinders their wider applications at the frame level. As a result, it is necessary to find alternatives that can achieve a rapid solution without sacrificing accuracies. To this end, shell elements and beam elements were preferred owing to the simplification in thickness and cross-section details. As shown in Fig. 7, parts of columns and beams were modelled with beam elements, while the regions close to beam-to-column connections were kept as solid elements in order to secure the precision of numerical results. The length of the beam with solid elements was equal to the beam depth since large stress concentrations were found within this region.

The tips of beam elements were bonded with the surfaces of solid elements via coupling constraints where six degrees of freedom were fixed. In addition, the concrete slab was replaced by the shell elements in which the geometrical centroid was offset to the bottom surface. The shell element also provided an option to include reinforcing bars by assigning area, space and position along the thickness direction. The shear connectors between the concrete slab and beam flanges were simulated with connector elements that were fixed in rotations, and the translations were related to the shear-resisting stiffness coefficients k_1 and k_2 as well as the pull-resisting stiffness coefficient k_3. The assumption could be reliable since almost all shear connectors remained elastic behaviour in the full shear configuration according to the numerical results of solid elements. For simplicity, the three shear stiffness coefficients were determined by a proposed formula from Lin *et al.* (2014).

$$k_{\mathrm{i}} = \frac{0.5V_{\mathrm{u}}}{(0.08-0.00086f_{\mathrm{c}})d_{\mathrm{s}}} \tag{8}$$

where f_c is the concrete compressive strength; d_s is the diameter of the headed stud; V_u is the shear strength for one headed stud which is taken as Eq. (9) according to EN 1994-1-1 (2004).

$$\text{Smaller of } \begin{cases} V_{\mathrm{u}} = 0.8\sigma_{\mathrm{us}}\pi d_{\mathrm{s}}^{2}/4 \\ V_{\mathrm{u}} = 0.29d_{\mathrm{s}}^{2}\sqrt{f_{\mathrm{c}}E_{\mathrm{c}}} \end{cases} \tag{9}$$

The results were then compared against those from solid elements, as indicated in Fig. 8. As for the load-displacement curves, the results obtained from the beam &

shell element model were reasonably consistent with the counterpart from the solid element model. The FEM-test result ratios related to the initial stiffness and ultimate resistance approached 1 and 1.07 respectively. It is noted that the displacement (Points B and C in Fig. 8(a)) corresponding to the ultimate resistance for two models was slightly inconsistent, which may be attributed to the difference of the shear connectors in the two models. Although the elastic response of shear connectors was observed in the solid element model, a pair of them adjacent to the middle column deformed evidently due to the local boundary effect. This could reduce the stiffness of joints at the final stage and then induced the bolts on endplates to sustain more loads which led to the eventual damage of bolts. On the other hand, the elastic performance was supposed for the connector elements simulating shear connectors in the shell element model, and their behaviour was not affected by the boundary effect. As such, the whole sub-model could undertake more loads. Nonetheless, the noncoincidence between Point B and Point C in Fig. 8(a) does not suggest the modelling method with beam and shell elements failed to be employed in this study since the progressive collapse response was investigated by the stage before Point B where the two curves agreed well. Additionally, with respect to the equivalent plastic strain of concrete slab, the distribution in shell elements was quite similar to that in solid element regardless of the local concentration due to the shear connector holes. As a result, the comparison also suggested the simplified modelling strategy was reasonably reliable to evaluate the structural performance under column removal scenarios.

3. Discussion on stainless steel joint sub-assemblages

Based on the verified finite element method, the composite joint sub-assemblage was further evaluated by assigning stainless steel material properties which are summarised in Table 1. It is noted that the constitutive model of stainless steel reinforcement was obtained from Gardner *et al.* (2016). The results of load-displacement relationship are plotted in Fig. 9. Meanwhile, for the purpose of classifying the primary component actions (force-controlled or deformation-controlled actions), a typical curve from UFC 4-023-03 (2009) was added in the figure highlighted in red. Point 2 corresponds to the ultimate resistance while Point 1 is critical since it determines the initial stiffness and hardening stiffness. As such, the strategy locating Point 1 was adopted from FEMA 356 (2000). The initial stiffness was firstly defined by the point corresponding to 60% of yield resistance (181.6 kN) which denoted the plastic strain of components reached 0.2%. The hardening stiffness was then confirmed by balancing the area in the actual curve (black line) and the idealised curve (red line) before Point 2. It can be seen that the load-deformation relationship of stainless steel composite joint complied with the trend of the typical curve, namely the resistance increased to the point where components experienced yielding followed by a strain-hardening enhancement, and then the structure could sustain additional loads by the residual capacity before the final failure. The provision also classified the level of performance by immediate occupancy, life safety and collapse prevention, and all levels for primary members should be limited within the range of strain-hardening enhancement according to the curve. Besides, since the displacement at Point 2 was more than two times that at Point 1, the structural form could be categorised as the deformation-controlled type which means the collapse prevention level could be evaluated based on the deformation acceptance criteria.

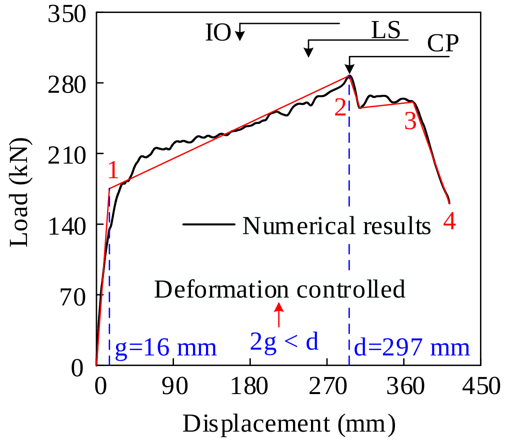

IO − Immediate Occupancy LS − Life Safety
CP − Collapse Prevention

Fig. 9 Load-displacement relationship of stainless steel beam-to-column joint sub-model

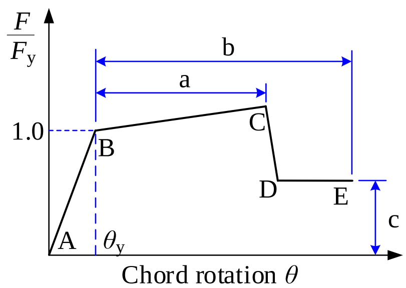

Fig. 10 Generalised load-deformation relationship for steel components

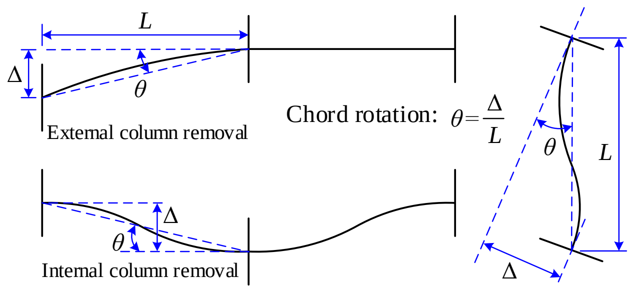

Fig. 11 Definition of chord rotation

Table 3 Properties of beam hinges, column hinges and connections

Component		Plastic rotation		Residual strength ratio	Acceptance criteria
		a	b	c	CP
Beam	$\frac{b_f}{2t_f} \le \frac{52}{\sqrt{\sigma_{ye}}}$ and $\frac{h}{t_w} \le \frac{418}{\sqrt{\sigma_{ye}}}$	$9\theta_y$	$11\theta_y$	0.6	$8\theta_y$
	$\frac{b_f}{2t_f} \ge \frac{65}{\sqrt{\sigma_{ye}}}$ or $\frac{h}{t_w} \ge \frac{640}{\sqrt{\sigma_{ye}}}$	$4\theta_y$	$6\theta_y$	0.2	$3\theta_y$
Column for $F/F_{ye} < 0.2$	$\frac{b_f}{2t_f} \le \frac{52}{\sqrt{\sigma_{ye}}}$ and $\frac{h}{t_w} \le \frac{300}{\sqrt{\sigma_{ye}}}$	$9\theta_y$	$11\theta_y$	0.6	$8\theta_y$
	$\frac{b_f}{2t_f} \ge \frac{65}{\sqrt{\sigma_{ye}}}$ or $\frac{h}{t_w} \ge \frac{460}{\sqrt{\sigma_{ye}}}$	$4\theta_y$	$6\theta_y$	0.2	$3\theta_y$
Column for $0.2 < F/F_{ye} < 0.5$	$\frac{b_f}{2t_f} \le \frac{52}{\sqrt{\sigma_{ye}}}$ and $\frac{h}{t_w} \le \frac{260}{\sqrt{\sigma_{ye}}}$	$11(1-1.7\frac{F}{F_{ye}})\theta_y$	$17(1-1.7\frac{F}{F_{ye}})\theta_y$	0.2	$11(1-1.7\frac{F}{F_{ye}})\theta_y$
	$\frac{b_f}{2t_f} \ge \frac{65}{\sqrt{\sigma_{ye}}}$ or $\frac{h}{t_w} \ge \frac{400}{\sqrt{\sigma_{ye}}}$	$1.0\theta_y$	$1.5\theta_y$	0.2	$0.8\theta_y$
Yield of endplate		0.042	0.042	0.8	0.035
Yield of bolts		0.018	0.024	0.8	0.015

Note: b_f and t_f is the width and thickness of flange, respectively; h and t_w is the clear depth and thickness of web, respectively; σ_{ye} is the yield strength of steel component; F_{ye} is the yield capacity; θ_y is the yield rotation.

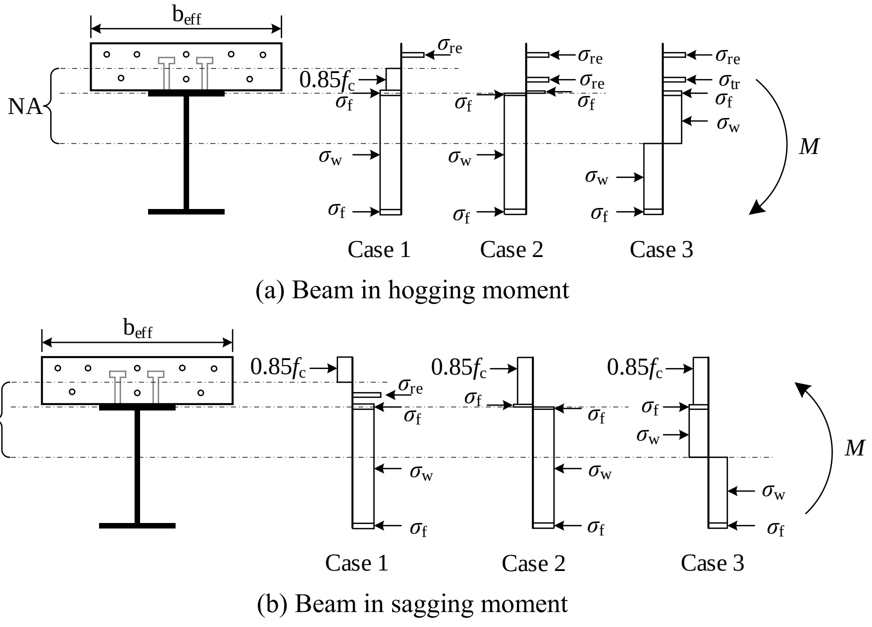

(a) Beam in hogging moment

(b) Beam in sagging moment

Fig. 12 Stress distribution diagrams in composite beams

The commonly used evaluation method for collapse prevention level was to develop frame models with beam elements and spring elements characterising beams, columns and connection zones. As for nonlinear static analysis, plastic hinges were expected to occur in beams and columns. Besides, plastic behaviour was considered for spring elements, provided the semi-continuous moment connections were used in frames. As a result, design guidance normally applied the generalised load-deformation relationships to plastic hinges and connections as shown in Fig. 10. Note that the chord rotation was defined as the ratio of relative deformations to the space between columns. Since the deformation-controlled type dominated the performance of semi-continuous frames, values of a and b in Fig. 10 could be of great importance to quantify the progressive collapse capacity. For example, whether a frame could be justified to possess sufficient collapse resistance relied on the acceptance criteria that shall be less than a or b of which the practical values were offered by design codes. It is noteworthy that these design codes only

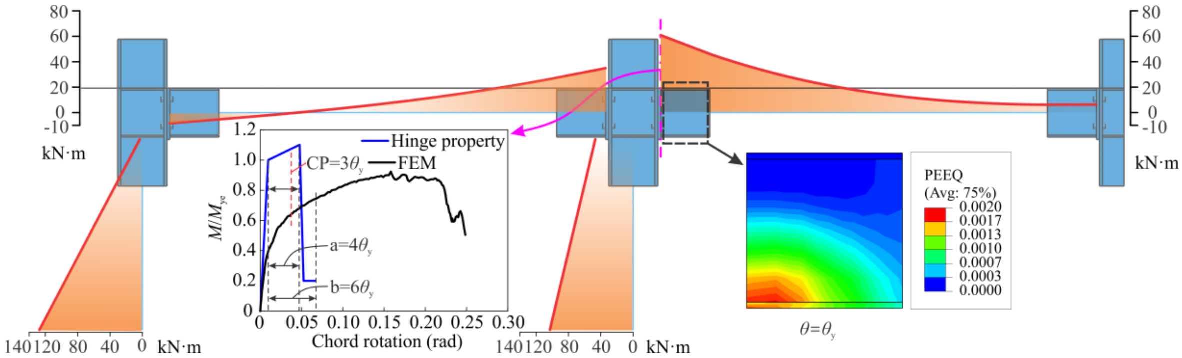

Fig. 13 Bending moment of sub-assemblage and moment-rotation relationship of composite beam

cover steel structures that differed from composite structures in terms of flexural response. As a result, one effort of this study was to explore the progressive collapse response and compared with design codes to assess if the practical values in provisions can be still feasible for stainless steel composite frames in nonlinear static analysis.

3.1 Flexural performance of beams and columns in sub-assemblages

UFC 4-023-03 (2009) adopted the design rules of FEMA 356 (2000) in terms of the generalised load-deformation relationships and acceptance criteria. The detailed information is outlined in Table 3. The yield rotation (θ_y) of beams and columns can be obtained by:

$$\theta_y = \frac{Z\sigma_{ye}L_b}{6EI_b} \tag{10}$$

$$\theta_y = \frac{Z\sigma_{ye}L_c}{6EI_c}\left(1-\frac{F}{F_{ye}}\right) \tag{11}$$

where Z is the plastic section modulus; σ_{ye} is the yield strength of steel components; L_b and L_c is the length of beam and column, respectively; I_b and I_c is the second moment of area of beam and column, respectively; F_{ye} is the yield force of steel member which is taken as $A\sigma_{ye}$.

As for composite beams in hogging and sagging moment, the parameters such as $Z\sigma_{ye}$ and EI_b should be obtained by taking composite actions into account, which can be achieved by the stress distribution patterns at the yielding stage illustrated in Fig. 12. The plastic neutral axis can be determined in accordance with force equilibrium which typically consists of three cases as shown, and the moment capacity ($Z\sigma_{ye}$) can be subsequently obtained. With respect to flexural stiffness (EI_b) in the sagging moment, the value can be determined by ANSI/AISC 360 (2016) in which the equivalent stiffness is provided by:

$$EI_{\rm b} = (EI)_{\rm equiv} = E_{\rm s}[I_{\rm s} + \sqrt{\Sigma V_{\rm n}/C_{\rm f}}\,(I_{\rm tr} - I_{\rm s})] \tag{12}$$

where I_s is the second moment of area of steel sections; I_{tr} is the second moment of area for the fully composite uncracked transformed section; $\sum V_n$ is the sum of shear capacity of shear connectors located from the maximum sagging moment to zero; C_f is the smaller value of $0.85f_cA_{con}$ and $A_s\sigma_{ye}$; f_c is the compressive strength of concrete slab; A_{con} is the section area of concrete slab within effective width; A_s is the section area of steel part. Note that $\sum V_n$ / C_f actually denotes the shear connection degree. I_{tr} can be defined based on the study by Faella *et al*. (2003) as

$$I_{\rm tr} = (I_{\rm s} + \alpha I_{\rm con}) + \frac{\alpha A_{\rm s} A_{\rm con}}{A_{\rm s} + \alpha A_{\rm con}} h_1^2 \tag{13}$$

where I_{con} is the second moment of area of concrete slab; α is the elastic modulus ratio which equals E_c/E_s; h_1 is the distance from the neutral axis of the concrete slab to the neutral axis of the steel section.

In addition, the flexural stiffness in the hogging moment can be adapted by replacing the contribution of the concrete slab with that of reinforcement. Therefore, Eq. (13) could be modified as:

$$I_{\rm tr} = (I_{\rm s} + I_{\rm re}) + \frac{A_{\rm s} A_{\rm re}}{A_{\rm s} + A_{\rm re}} h_1^2 \tag{14}$$

where I_{re} and A_{re} is the second moment of area and cross-section area of reinforcement, respectively.

The bending moment diagram of the sub-model corresponding to maximum hogging moment is illustrated in Fig. 13. It could be seen that the absolute value of sagging moment was much smaller than that of hogging moment. Therefore, only the beam region under hogging moment was assessed in terms of moment-rotation relationship as plotted in Fig. 13. Note that although the beam experienced large rotations, the bending moment was still lower than the yielding resistance calculated from Fig. 12. It is to be expected since the flexural moments at the end of the beam were dominated by the beam-to-column connections. As a result, the actual moment-rotation relationship significantly differed from the hinge property of beams. As shown in Fig. 13, the yield rotation of composite beams approached 0.0041 in accordance with design codes while the numerical model corresponding to this rotation did not thoroughly exhibit yielding performance based on the PEEQ distribution. Moreover, the deflection limit for collapse prevention was too small compared to the FEM results which may lead to an over-conservative design for stainless steel structures. It is noteworthy that the progressive collapse behaviour of the joint sub-model was explored by the displacement-

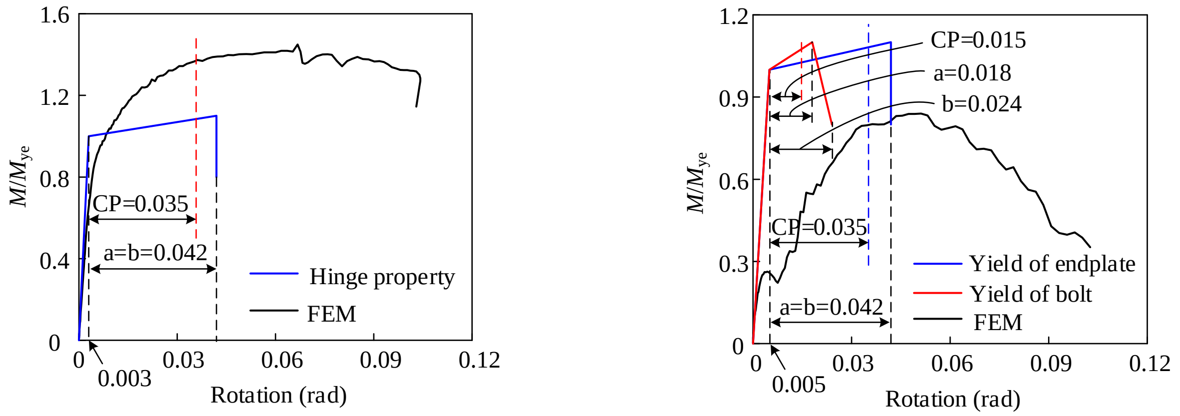

(a) Connections in hogging moment region (b) Connections in sagging moment region

Fig. 14 Moment-rotation relationship of connections

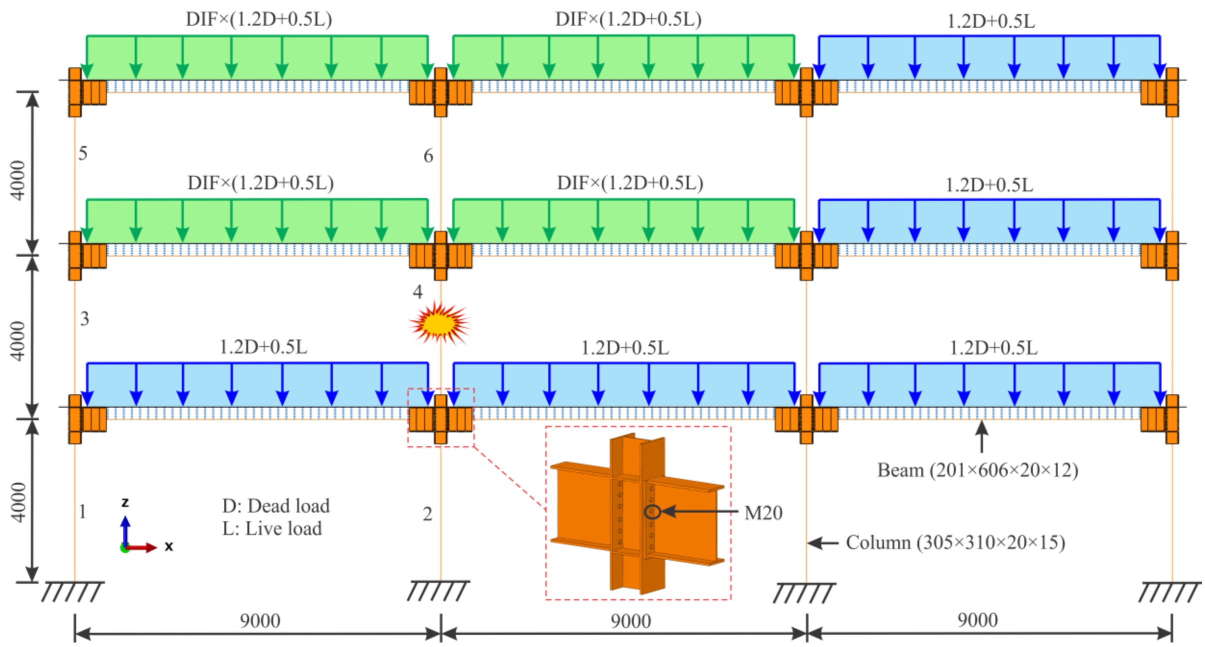

Fig. 15 Frame layout under column removal scenario (Unit: mm)

controlled strategy, more attention would thus be paid on rotations.

With respect to columns, the bending moments basically retained the elastic properties, and thus the moment-rotation response was not discussed in this section. More detailed assessment was performed in Section 4.

3.2 Flexural performance of connections in sub-assemblages

The moment-rotation behaviour of beam-to-column connections in hogging and sagging moment regions is depicted in Fig. 14. The hogging yielding moment resistance was obtained based on the method proposed by Song *et al*. (2019), while the sagging one can be acquired by EN 1993-1-8 (2005). Meanwhile, the hinge properties were also determined by UFC 4-023-03 (2009) where the yielding rotation corresponding to the yielding moment was suggested as 0.005 for the sagging region and 0.003 for the hogging region as a result of the contribution from reinforcing bars.

It can be seen from Fig. 14(a) that although the design limit of collapse prevention (0.035) in UFC 4-023-03 exceeded 0.03 which is the typical boundary for seismic design of buildings, the value was far less than the rotation capacity of stainless steel joints (around 0.1), and this hindered the potential advantages of stainless steel structures such as high ductility and large strain-hardening effects. Similarly, a conservative design was observed in the connections under sagging moment where bolts or endplate experienced yielding. Note that the maximum moment for connections under the sagging moment was smaller than the yielding moment resistance predicted by design codes, in which the ratio of the former to the latter can approach 0.84.

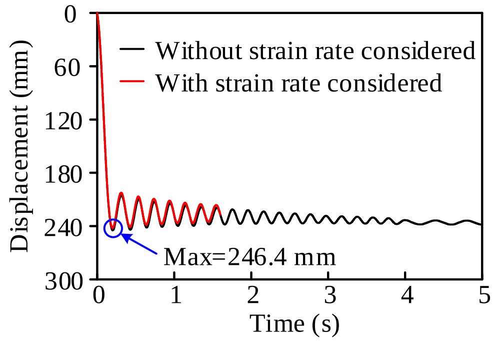

(a) Removal of Column 2

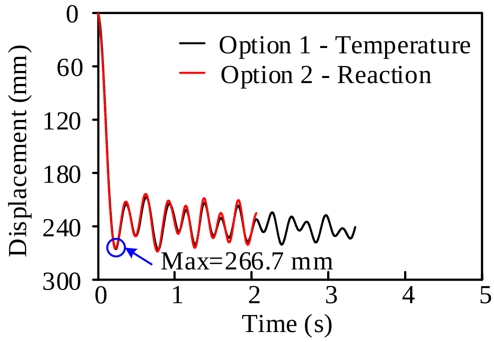

(b) Removal of Column 3

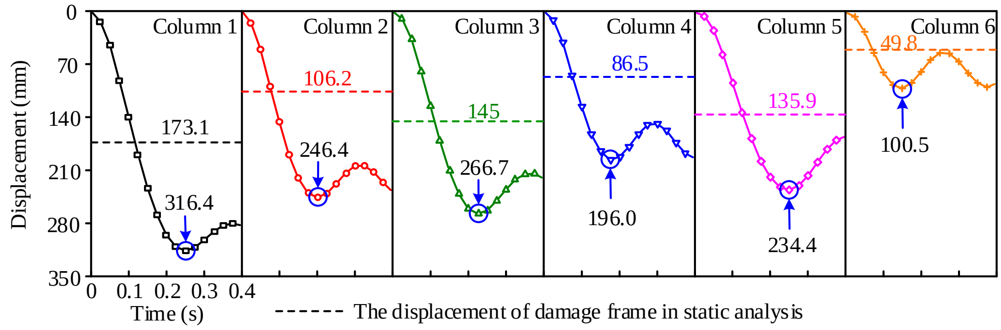

(c) Removal of Columns 1-6

Fig. 16 Displacement response of frames under a column removal scenario

This is attributed to the effect of catenary actions leading to the large tensile forces applied to the connection under the sagging moment, and this could induce the premature failure of bolts or yielding of the endplate in bending. In this light, more focus should be taken on these regions to improve the robust performance of composite frames under a column removal scenario.

4. Frame analysis under column removal scenario

The dynamic increase factor (DIF) needs to be re-assessed for stainless steel composite frames which can only be achieved at the frame level. To this end, a three-bay by three-story frame with the span of 9000 mm and the storey height of 4000 mm was designed as shown in Fig. 15. The width, depth, thickness of flange and web of universal columns and beams were 305×310×20×15 mm and 201×606×20×12 mm, respectively. Since the beam-to-column connections under sagging moment were critical, especially when they were subjected to large tensions due to catenary actions, M20 stainless steel bolts were deployed with six rows to achieve sufficient resistances. The 120 mm thick concrete slabs were deployed of which the width was larger than the effective width. The modelling strategy was similar to the sub-models combining beam elements, shell elements and solid elements to save computation costs, and the details were not repeated herein. Only dead loads and live loads were considered in accordance with UFC 4-023-03 (2009), and the design values were obtained from AS/NZS 1170.1 (2002). Accordingly, the dead loads were determined by self-weights of components and distributed to the concrete slab at each span. The relatively high live loads characterising offices and work areas were defined in order to assess the potential performance of stainless steel composite frames to extreme extents. As such, the distributed and concentrated actions for working levels were 5 kPa and 4.5 kN respectively, while those for roof were taken as 0.25 kPa and 1.1 kN respectively. The load combinations were acquired as

$$L_{\text{comb}} = 1.2D + 0.5L \tag{15}$$

where D and L denote dead loads and live loads, respectively.

Nonlinear dynamic and static analysis could be separately performed for each column in terms of progressive collapse behaviour. As per UFC 4-023-03 (2009), the four steps for determining DIF are:

Step 1: Performing quasi-static analysis for the intact frame to obtain the initial stress and strain field before collapse which is simulated by Step 2. Note that the unamplified load combinations should be applied;

Step 2: Performing dynamic analysis by releasing the constraints of one column instantaneously to acquire the deflection response of the frame in which the maximum displacement can be recorded;

Step 3: Calculating the maximum ratio of plastic rotation to yield rotation in dynamic analysis for damaged frames. The yield rotation of beams and columns is taken as Eqs. (10) and (11), while that of joints is set as 0.003 and

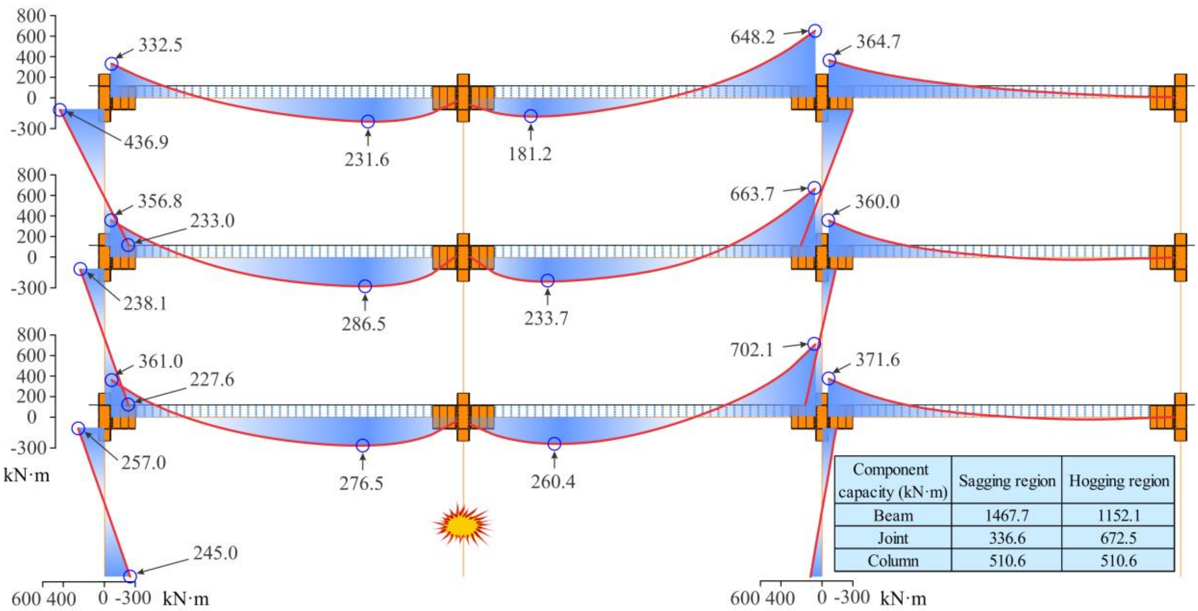

Component capacity (kN·m)	Sagging region	Hogging region
Beam	1467.7	1152.1
Joint	336.6	672.5
Column	510.6	510.6

Fig. 17 Bending moment diagram of frames under the removal of Column 2

0.005 for hogging and sagging moment regions respectively;

Step 4: Performing pushdown analysis by amplifying the load combinations directly above the removed column to find out an appropriate DIF where the displacement matches that in dynamic analysis corresponding to the maximum ratio found by Step 3.

4.1 Nonlinear dynamic analysis

The nonlinear dynamic analysis could straightforwardly reflect the real progressive collapse response of structures. In this study, the dynamic analysis was also performed by the dynamic/explicit solver in Abaqus software. The typical procedure included two steps as mentioned above (Steps 1 and 2), namely the quasi-static analysis and dynamic analysis. The first step aimed to obtain the initial status of the frame under the original load combination before column removal. Note that the load combination was intentionally taken as 1.2D+0.5L without the dynamic increase factor considered. Subsequently, one of the columns (from Column 1 to Column 6) was deactivated instantaneously, and the frame response was updated based on the internal force equilibrium. The removal of the columns at ground level (Columns 1 and 2 shown in Fig. 15) was achieved by deactivating the boundary conditions of the column end. Apart from that, the upper-story columns could be removed in two options, namely introducing temperature field strategy or applying reactions to the damaged frame. As for the temperature field strategy, the affected column was assigned with special material properties where temperature-dependent stress-strain relationships were adopted. The constitutive model under ambient temperature remained identical while the yield stress at a higher temperature such as 50°C was reduced to near zero. Once the dynamic analysis commenced, the high temperature was only applied to the removed column within a short period (0.01s). Consequently, the column could notsustain the original resistance anymore which was equivalent to the removal scenario. Additionally, the reaction method that has been used by Liu (2013) and Zhu *et al*. (2018) could provide an alternative option. By this means, the internal forces of a column were firstly obtained from the quasi-static analysis of the complete frame, and then in the damaged frame, the forces were added to the same position where the column has been deleted. Afterwards, a new quasi-static analysis was performed to obtain the stress and strain field. Last, the added forces were deactivated for the dynamic simulation. The two methods would be discussed and compared later.

It is noteworthy that the dynamic analysis could induce a relatively high strain rate to steel components which may also result in enhanced stress behaviour (Cai and Young 2019, Lichtenfeld *et al*. 2006). In this case, strain-rate-dependent constitutive models were expected to be taken into account. The Cowper-Symonds overstress power law was herein adopted owing to its simplicity, and the expression can be

$$\bar{\sigma} = \sigma^0 R \tag{16}$$

$$R = 1 + (r / M)^{1/p} \tag{17}$$

where σ^0 is the static stress; R is the overstress amplification factor related to strain rates; r is the strain rate; M and p are material parameters.

Due to a lack of experimental material properties at various strain rates, the data from previous study (Lichtenfeld *et al*. 2006) was used to determine the material parameters D and p via regression analysis, which was 2826 and 5.06 respectively. The calibrated strain rates ranged from 0.000125 s^{-1} to 400 s^{-1} which could cover the dynamic effects under the column removal scenario.

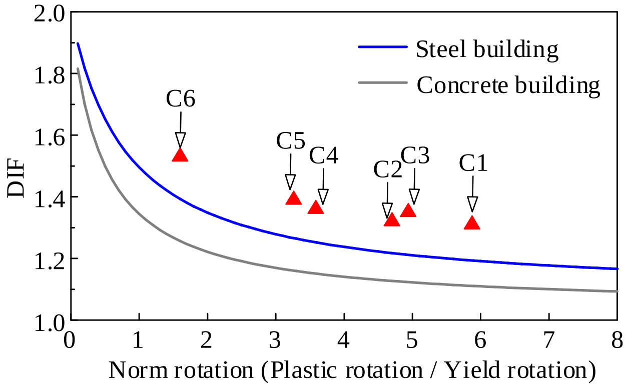

Fig. 18 Comparison of DIF between numerical results and design guidance

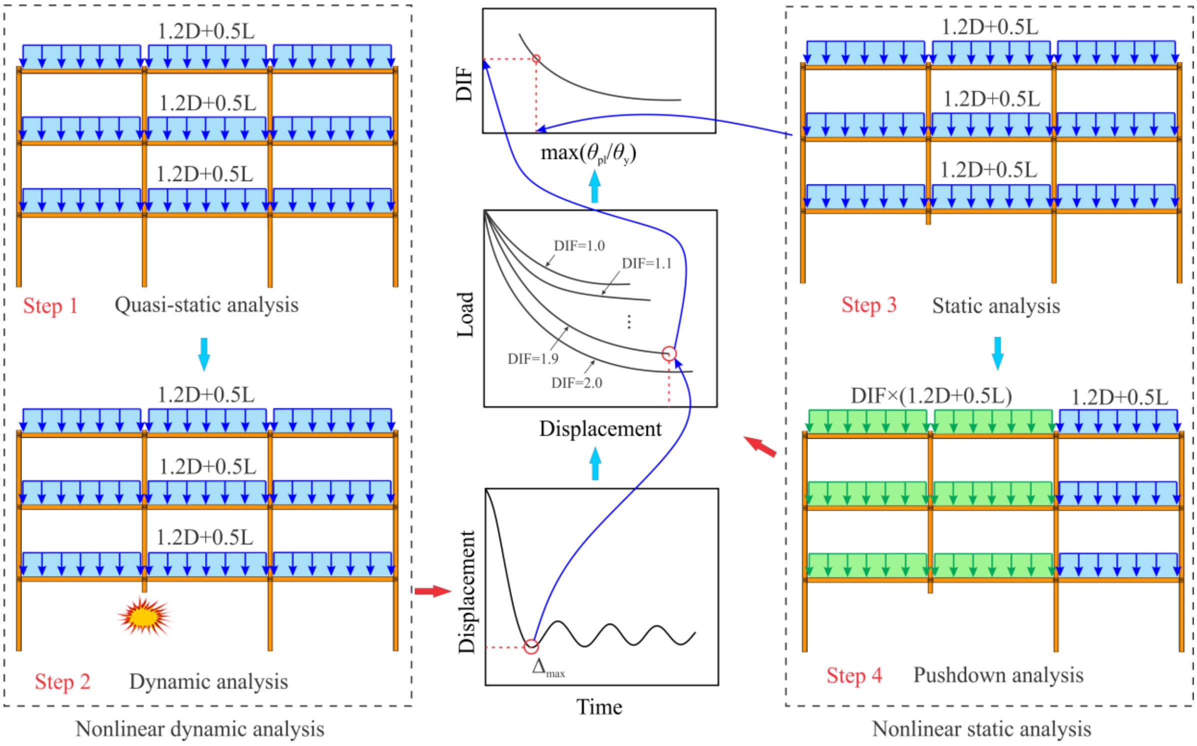

Fig. 19 Flowchart determining DIF for frames

The displacement responses of the frame with an arbitrary column removed are displayed in Fig. 16 where the displacement was taken from a point of the solid element directly adjacent to the top of removed column. As a typical example of demonstration (Column 2 removal), it can be seen in Fig. 16(a) that the frame experienced a large deformation immediately after the column removal, followed by damped oscillations until it approached stability due to the effect of catenary actions that were able to prevent composite frames from the severe collapse. The effect of strain rate was preliminarily assessed by comparing the frame responses, and it is suggested that the influence can be ignored since the large strain rate only occurred in bolts between endplates and columns. Nonetheless, to assure the accuracy of results, all dynamic analysis had considered the strain rate effects. Concerning the two methods of modelling column removal, it can be seen in Fig. 16(b) that the two options provided almost identical predictions. This demonstrated that the temperature field method was feasible to achieve the effect of column loss, and moreover the short time used in the method was reasonable to reflect the strain rate effects in practical structural engineering problems. Although both methods can provide satisfactory results, the option using temperature field could be more convenient since there is no need to record or export the reactions in static analysis to the dynamic analysis. As such, the following frame analysis adopted the method with temperature to simulate the column removal. Fig. 16(c) illustrates the displacement response of frame under the corresponding column removal scenarios. Comparing the maximum displacements, it is found that the frame could be more vulnerable to the progressive collapse under the removal of external column which was only braced by one-side beams. The dash line in Fig. 16(c) denotes the displacement of damaged frame under unamplified loading conditions (1.2D+0.5L) in static analysis. Note that the ratio of the peak in dynamic analysis to the value in static analysis ranged from 1.7 to 2.3, and this is the direct reason why the dynamic increase factor was previously taken as 2 in design guidance which ignored the contribution of catenary actions and also the strain-hardening effects in stainless steels.

Additionally, the bending moment distribution of composite frame corresponding to the maximum deformation in dynamic analysis is plotted in Fig. 17. The diagram is expected to locate the critical position that dominates the maximum ratio of plastic rotation to yield rotation. The moment capacity of beams, columns and joints could be obtained based on AS/NZS 2327 (2017) and EN 1993-1-8 (2005). It can be seen that the joints in hogging moment regions experienced significant flexural response which exceeded the moment capacity of joints, while beams and columns retained within the moment capacity. Accordingly, more attention need to be paid to the critical position to locate the maximum ratio of plastic rotation to yield rotation under this column removal scenario.

4.2 Nonlinear static analysis

As mentioned above, the dynamic increase factor cannot be directly obtained by the static analysis under unamplified loading conditions. Instead, it is required to find out the appropriate DIF by applying a series of amplification values to the damaged frame in static analysis until the displacement matched the peak deformation in dynamic analysis with acceptable accuracy. Finally, the relationship between DIF and the norm rotation (ratio of plastic rotation to yield rotation) can be summarised for all column removal scenarios, which has been plotted in Fig. 18. Note that the yield rotation of beams and columns can be determined by Eqs. (10) and (11), while that of joints could be simply taken as 0.003 and 0.005 for hogging and sagging moment region, respectively, according to UFC 4-023-03. As suggested by McKay (2008), the plastic rotation can be defined as

$$\theta_{\mathrm{pl}} = \theta_{\mathrm{cal}} - \theta_{\mathrm{y}} \tag{18}$$

where θ_{pl} is the plastic rotation, θ_{y} is the yield rotation, θ_{cal} is the total rotation of beams, columns or joints in dynamic analysis and it can be calculated based on Fig. 11 for beams and columns or based on the rotation of endplates for joints.

It is found from Fig. 18 that the joints generally dominated the definition of norm rotation, which can be deemed as the most vulnerable components in a typical frame. Besides, the design provisions recommended by UFC 4-023-03 were collected and compared with the values for stainless steel buildings. It can be seen that it is non-conservative to directly adopt the current guidance for the progressive collapse design of stainless steel composite frames. It is to be expected since the ductility of stainless steel is higher than mild steel resulting in larger plastic rotations. In this light, a new relationship between DIF and norm rotation for stainless steel composite frames should be derived through regression analysis from a wide range of databases.

5. Design recommendations for DIF

This study firstly outlined the specific procedure that could systematically determine the DIF-norm rotation curve, which was adapted from UFC 4-023-03 (2009). The flowchart is illustrated in Fig. 19 and detailed steps were similar as mentioned in Section 4, except Step 3 where static analysis of damaged frames was performed to determine the norm rotation for simplicity. Note that the yield rotation of joints was still defined as 0.003 and 0.005 for hogging and sagging moment regions respectively given that engineers could readily determine the norm rotation without calculating case by case. The frame with three stories and three bays was re-assessed by the new steps, and moreover, a nine-story by five-bay composite frame model was established to obtain more results as illustrated in Fig. 20.

The numerical results were collected and plotted in Fig. 21 in terms of DIF-norm rotation relationships. It can be seen that the DIF value slightly increased within the large norm rotation range which is evidently different from the typical curve in UFC 4-023-03 (2009). This could be attributed to the high ductility of stainless steel, allowing frames to develop more catenary actions. Based on these data, a new fitting curve was derived via regression analysis. Meanwhile, the upper and lower bound prediction curves were provided which covered all DIF values. Note that the discrepancies between the upper bound prediction curve and the fitting curve was not significant, to confidently predict DIF values, the upper bound prediction curve was proposed as the design recommendations for DIF

$$\mathrm{DIF} = 1.220 + \frac{0.307}{\theta_{\mathrm{pl}} / \theta_{\mathrm{y}} + 0.349} + 0.00882(\theta_{\mathrm{pl}} / \theta_{\mathrm{y}}) \tag{19}$$

Once DIF-norm rotation curve was defined, in engineering practice, designers could assess the progressive collapse performance of stainless steel composite frames by means of nonlinear static analysis which saved time and reduced labour costs. The updated scheme is illustrated in Fig. 22 and summarised as:

Step 1: Performing nonlinear static analysis on damages frames with unamplified loading (1.2D+0.5L). Determining the norm rotations of members (beams, columns and joints) above the removed column. Note that the plastic rotation herein is the difference between the total rotation from nonlinear static analysis and the yield rotation.

Step 2: Finding out DIF corresponding to the minimum norm rotation under the column removal scenario and performing nonlinear static analysis on damaged frames with amplified loading (DIF×(1.2D+0.5L)).

Step 3: Comparing all plastic rotations of components with the acceptance criteria in turn to justify if the component capacity satisfies the requirements. Repeating the process for other removed columns until all criteria have

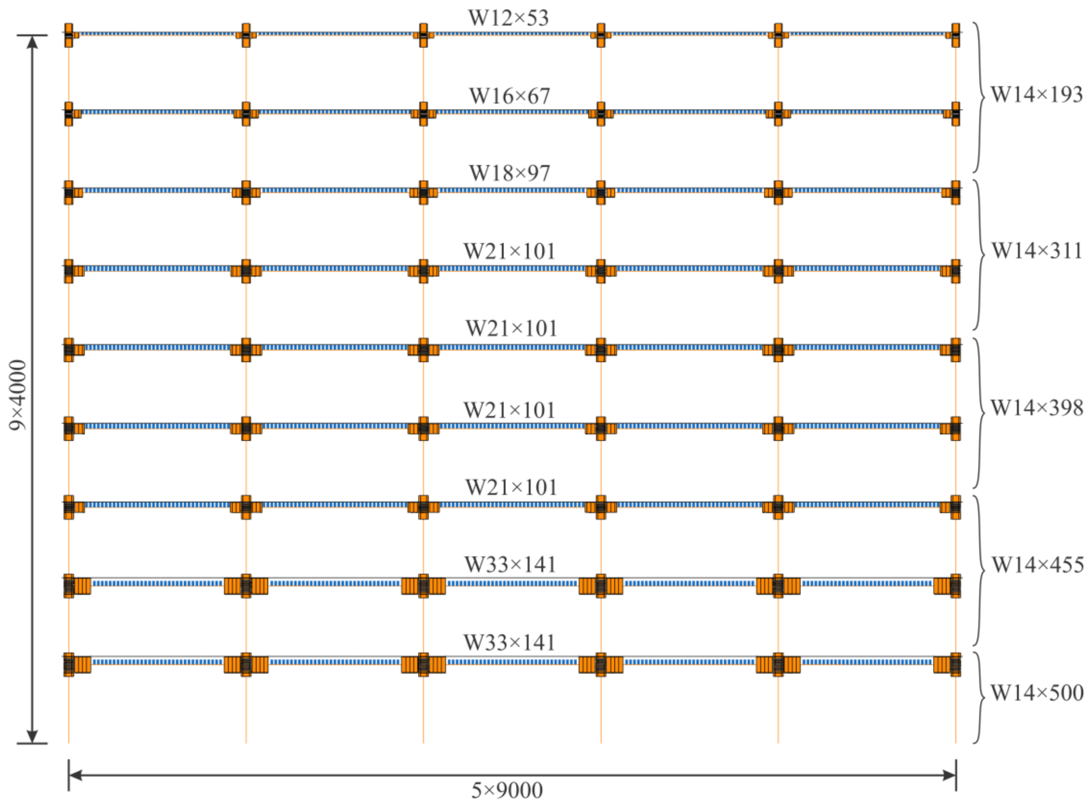

Fig. 20 Configuration of composite frame

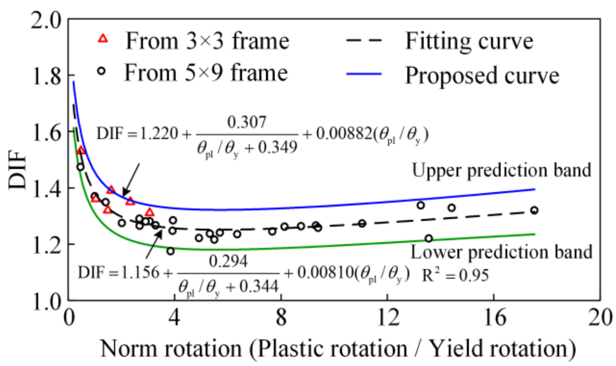

Fig. 21 Design recommendation for DIF

been satisfied.

The proposed method simplifies the progressive collapse design procedure and is compatible with current design guidance regarding mild steel structures. In this case, it could be promising to provide straightforward design guidance for stainless steel composite frame buildings.

6. Conclusions

The progressive collapse performance of stainless steel composite structures has been numerically investigated in sub-assemblage and frame levels which were validated by independent experimental results. The flexural response has been comprehensively assessed in terms of moment-rotation relationships, plastic hinges and catenary actions. The dynamic increase factor (DIF) has been evaluated based on design guidance and the modified design process has been clarified. Some crucial conclusions are herein drawn:

- The simplified modelling strategy replacing parts of solid elements with shell, beam and connector elements was demonstrated to be reliable to predict the flexural performance of beam-to-column composite joint sub-assemblages.
- The stainless steel beam-to-column composite joint sub-models were classified as deformation-controlled design, but the provision of plastic hinges for beams cannot dominate the design of semi-continuous joints. The rotation acceptance criteria of beams and joints for collapse prevention were significantly conservative for stainless steel structures.

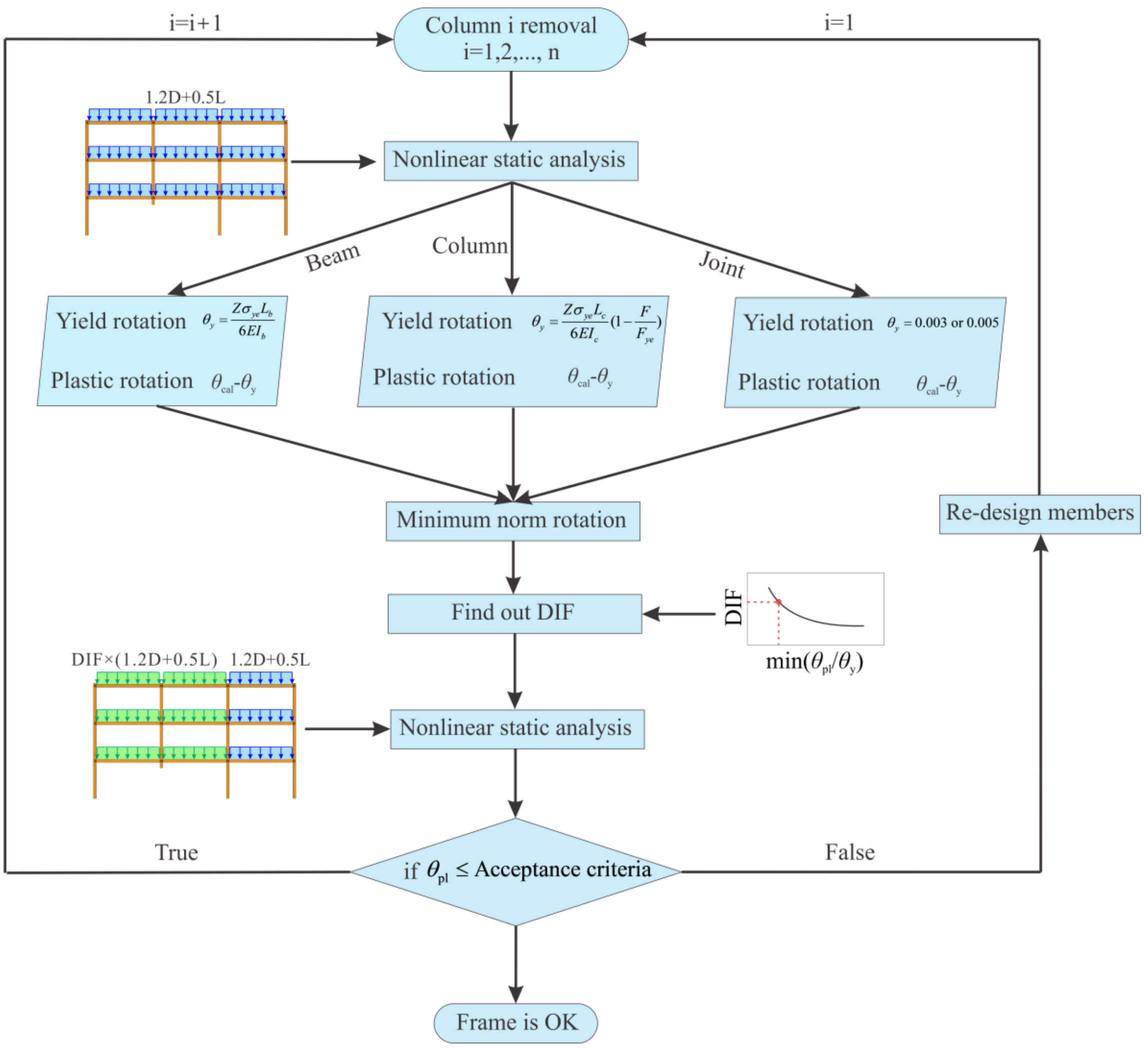

Fig. 22 Progressive collapse design process for stainless steel composite frames

- Catenary actions played an import role in the progress collapse performance, which could induce additional tensions to the connection in sagging moment. As such, the tensions would result in premature failure of bolts or yielding of the endplates in bending, and the regions need more attention to achieve robust design capacity.
- The deformation response in dynamic analysis suggested that the deformation is remarkably higher than that in static analysis, but the stainless steel composite frame can sustain the column-removal-induced actions through significant strain-hardening effects and catenary actions which allow the damaged members to bridge over columns. Besides, the structure could be more vulnerable under the external column removal scenarios leading to larger deflections.
- The beam-to-column joint in hogging moment is the major position that governs the determination of norm rotation (the ratio of plastic rotation to yield rotation). The current design guidance is non-conservative to define DIF for stainless steel composite frames.
- A modified procedure determining the DIF-norm rotation curve is proposed based on the previous design codes and the corresponding curve is derived via regression analysis. The specific step for defining norm rotation is clarified by collecting the plastic rotation from static analysis instead of dynamic analysis.

A major challenge for collapse prevention design of stainless steel composite frames is to develop a rational and reliable DIF-norm rotation curve, which requires a large number of database involving various geometrical details and structural forms. Accordingly, more works on determining DIF following the proposed flowchart are suggested to verify the application of the design curve and consequently promote the development of stainless steel structures in engineering practice.

Acknowledgments

The research described in this paper is financially supported by the Australian Research Council (ARC) under its Discovery Scheme (Project No: DP180100418). The financial support is gratefully acknowledged. The authors acknowledge the University of Sydney HPC service for providing resources that have contributed to the research results in this paper.

References

ABAQUS (2016), User Manual. Version 6.16, DS SIMULIA Corp, Providence, RI, USA.

ANSI/AISC 360 (2010), Specification for structural steel buildings, American Institute of Steel Construction; Chicago-Illinois, USA.

AS 4100 (1998), Steel Structures, the Council of Standards Australia; Sydney, Australia.

ASCE/SEI 41-17 (2017), Seismic evaluation and retrofit of existing buildings. American Society of Civil Engineers; Virginia, USA.

AS/NZS 1170.1 (2002), Structural design actions Part 1: Permanent, imposed and other actions, the Council of Standards Australia; Sydney, Australia.

AS/NZS 2327 (2017), Composite structures—Composite steel-concrete construction in buildings, the Council of Standards Australia; Sydney, Australia.

Cai, Y. and Young, B. (2019), "Experimental investigation of carbon steel and stainless steel bolted connections at different strain rates", *Steel Compos. Struct.*, **30**(6), 551-565. https://doi.org/10.12989/scs.2019.30.6.551.

Carreira, D.J. and Chu, K.H. (1985), "Stress-strain relationship for plain concrete in compression", *J. Proceedings*, **82**(6), 797-804.

Cassiano1a, D., D'Aniello, M., Rebelo, C., Landolfo, R. and da Silva, L.S. (2016), "Influence of seismic design rules on the robustness of steel moment resisting frames", *Steel Compos. Struct.*, **21**(3), 479-500. https://doi.org/10.12989/scs.2016.21.3.479.

Chen, J., Huang, X., Ma, R. and He, M. (2012), "Experimental study on the progressive collapse resistance of a two-story steel moment frame", *J. Perform. Constr. Fac.*, **26**(5), 567-575. https://doi.org/10.1061/(ASCE)CF.1943-5509.0000287.

Elflah, M., Theofanous, M., Dirar, S. and Yuan, H. (2019), "Behaviour of stainless steel beam-to-column joints—Part 1: Experimental investigation", *J. Constr. Steel Res.*, **152**, 183-193. https://doi.org/10.1016/j.jcsr.2018.02.040.

EN 1993-1-8 (2005), Eurocode 3: Design of steel structures — Part 1-8: Design of joints, European Committee for Standardization; Brussels, Belgium.

EN 1994-1-1 (2004), Eurocode 4: Design of composite steel and concrete structures — Part 1-1: General rules and rules for buildings, European Committee for Standardization; Brussels, Belgium.

Faella, C., Martinelli, E. and Nigro, E. (2003), "Shear connection nonlinearity and deflections of steel–concrete composite beams: a simplified method", *J. Struct. Eng.*, **129**(1), 12-20. https://doi.org/10.1061/(ASCE)0733-9445(2003)129:1(12).

FEMA 356 (2000), Prestandard and commentary for the seismic rehabilitation of buildings, American Society of Civil Engineers; Virginia, USA.

Gardner, L., Bu, Y., Francis, P., Baddoo, N.R., Cashell, K.A. and McCann, F. (2016), "Elevated temperature material properties of stainless steel reinforcing bar", *Constr. Build. Mater.*, **114**, 977-997. https://doi.org/10.1016/j.conbuildmat.2016.04.009.

GSA (2003), Progressive collapse analysis and design guidelines for new federal office buildings and major modernization projects, U.S. General Services Administration; Washington, D.C., USA.

Guo, L., Gao, S. and Fu, F. (2015), "Structural performance of semi-rigid composite frame under column loss", *Eng. Struct.*, **95**, 112-126. https://doi.org/10.1016/j.engstruct.2015.03.049.

Li, G.Q., Li, L.L., Jiang, B. and Lu, Y. (2018), "Experimental study on progressive collapse resistance of steel frames under a sudden column removal scenario", *J. Constr. Steel Res.*, **147**, 1-15. https://doi.org/10.1016/j.jcsr.2018.03.023.

Lichtenfeld, J.A., Van Tyne, C.J. and Mataya, M.C. (2006), "Effect of strain rate on stress-strain behavior of alloy 309 and 304L austenitic stainless steel", *Metallurgical Mater. T. A*, **37**(1), 147-161. https://doi.org/10.1007/s11661-006-0160-5.

Lin, Z., Liu, Y. and He, J. (2014), "Behavior of stud connectors under combined shear and tension loads", *Eng. Struct.*, **81**, 362-376. https://doi.org/10.1016/j.engstruct.2014.10.016.

Liu, M. (2013), "A new dynamic increase factor for nonlinear static alternate path analysis of building frames against progressive collapse", *Eng. Struct.*, **48**, 666-673. https://doi.org/10.1016/j.engstruct.2012.12.011.

Mashhadi, J. and Saffari, H. (2016), "Effects of damping ratio on dynamic increase factor in progressive collapse", *Steel Compos. Struct.*, **22**(3), 677-690. https://doi.org/10.12989/scs.2016.22.3.677.

McKay, A. (2008), "Alternative path method in progressive collapse analysis: Variation of dynamic and non-linear load increase factors", M.S. Dissertation, The University of Texas, San Antonio.

McKay, A., Marchand, K. and Diaz, M. (2012), "Alternate path method in progressive collapse analysis: Variation of dynamic and nonlinear load increase factors", *Practice Periodical on Structural Design and Construction*, **17**(4), 152-160. https://doi.org/10.1061/(ASCE)SC.1943-5576.0000126.

Mirtaheri, M. and Zoghi, M.A. (2016), "Design guides to resist progressive collapse for steel structures", *Steel Compos. Struct.*, **20**(2), 357-378. https://doi.org/10.12989/scs.2016.20.2.357.

Pavlović, M., Marković, Z., Veljković, M. and Buđevac, D. (2013), "Bolted shear connectors vs. headed studs behaviour in push-out tests", *J. Constr. Steel Res.*, **88**, 134-149. https://doi.org/10.1016/j.jcsr.2013.05.003.

Sadek, F., Main, J.A., Lew, H.S. and Bao, Y. (2011), "Testing and analysis of steel and concrete beam-column assemblies under a column removal scenario", *J. Struct. Eng.*, **137**(9), 881-892. https://doi.org/10.1061/(ASCE)ST.1943-541X.0000422.

Song, Y., Uy, B. and Wang, J. (2019), "Numerical analysis of stainless steel-concrete composite beam-to-column joints with bolted flush endplates", *Steel Compos. Struct.*, **33**(1), 143-162. https://doi.org/10.12989/scs.2019.33.1.143.

UFC 4-023-03 (2009), Design of buildings to resist progressive collapse. Unified Facilities Criteria, U.S. Department of Defense; Washington, D.C., USA.

Wang, J., Uy, B. and Li, D. (2019), "Behaviour of large fabricated stainless steel beam-to-tubular column joints with extended endplates", *Steel Compos. Struct.*, **32**(1), 141-156. https://doi.org/10.12989/scs.2019.32.1.141.

Wang, J., Uy, B., Thai, H.T. and Li, D. (2018a), "Behaviour and design of demountable beam-to-column composite bolted joints with extended end-plates", *J. Constr. Steel Res.*, **144**, 221-235. https://doi.org/10.1016/j.jcsr.2018.02.002.

Wang, J., Zhu, H., Uy, B., Patel, V., Aslani, F. and Li, D. (2018b), "Moment-rotation relationship of hollow-section beam-to-column steel joints with extended end-plates", *Steel Compos. Struct.*, **29**(6), 717-734. https://doi.org/10.12989/scs.2018.29.6.717.

Xu, M., Gao, S., Guo, L., Fu, F. and Zhang, S. (2018), "Study on collapse mechanism of steel frame with CFST-columns under column-removal scenario", *J. Constr. Steel Res.*, **141**, 275-286. https://doi.org/10.1016/j.jcsr.2017.11.020.

Yang, B. and Tan, K.H. (2013), "Experimental tests of different types of bolted steel beam–column joints under a central-column-removal scenario", *Eng. Struct.*, **54**, 112-130. https://doi.org/10.1016/j.engstruct.2013.03.037.

Yang, B., Tan, K.H. and Xiong, G. (2015), "Behaviour of composite beam–column joints under a middle-column-removal scenario: Component-based modelling", *J. Constr. Steel Res.*, **104**, 137-154. https://doi.org/10.1016/j.jcsr.2014.10.003.

Yang, B., Tan, K.H., Xiong, G. and Nie, S.D. (2016), "Experimental study about composite frames under an internal column-removal scenario", *J. Constr. Steel Res.*, **121**, 341-351. https://doi.org/10.1016/j.jcsr.2016.03.001.

Zhu, Y.F., Chen, C.H., Yao, Y., Keer, L.M. and Huang, Y. (2018), "Dynamic increase factor for progressive collapse analysis of semi-rigid steel frames", *Steel Compos. Struct.*, **28**(2), 209-221. https://doi.org/10.12989/scs.2018.28.2.209.

DL

Notations

A_{con}	Cross-section area of concrete slab with effective width
A_{re}	Cross-section area of reinforcement
A_s	Cross-section area of steel component
C_f	Smaller value of $0.85f_cA_{con}$ and $A_s\sigma_{ye}$
D and L	Dead load and live load
E_c	Young's modulus of concrete
E_0 and E_s	Young's modulus of steel
F	Compression of column
F_{ye}	Yield force of steel column which is taken as $A\sigma_{ye}$
I_b	Second moment of area of beam
I_c	Second moment of area of column
I_{con}	Second moment of area of concrete slab
I_{re}	Second moment of area of reinforcement
I_s	Second moment of area of steel section
L_b and L_c	Length of beam and column
L_E	Characteristic element length
M and p	Material parameters related to strain rates
R	Overstress amplification factor related to strain rates
V_n	Shear strength for headed stud
Z	Plastic section modulus
b_{eff}	Effective width of concrete slab
b_f and t_f	Width and thickness of flange
d_s	Diameter of headed stud
f_c	Compressive strength of concrete
h and t_w	Clear depth and thickness of web
h_1	Distance from neutral axis of concrete slab to neutral axis of steel section
k_1, k_2, k_3	shear-resisting stiffness coefficients and pull-resisting stiffness coefficient
m and n	Exponents related to strain hardening
r	Strain rate
$\bar{u}_f^{pl}$	Equivalent plastic displacement at fracture
α	Elastic modulus ratio which equals E_c/E_s
ε_c	Strain corresponding to compressive strength of concrete
ε_u	Ultimate strain corresponding to ultimate strength of steel
$\varepsilon_{0.2}$, $\sigma_{0.2}$	Strain and stress corresponding to plastic strain of 0.002
ε_d^{pl}	Equivalent plastic strain at the onset of damage
ε_f^{pl}	Equivalent plastic strain at fracture
θ	Stress triaxiality
θ_{cal}	Total rotation of member from FEM
θ_{pl}	Plastic rotation of member
θ_y	Yield rotation of member
λ	Element size factor
σ_{re}	Yield stress in reinforcement
σ_u	Ultimate strength of steel
σ_{us}	Tensile strength of shear connector
σ_{ye}	Yield strength of steel component
σ^0	Static stress
$\sum V_n$	Sum of shear capacity of shear connectors located from maximum sagging moment to zero